

# Genome-wide CRISPR screens reveal a Wnt–FZD5 signaling circuit as a druggable vulnerability of *RNF43*-mutant pancreatic tumors

Zachary Steinhart<sup>1</sup>, Zvezdan Pavlovic<sup>2</sup>, Megha Chandrashekhar<sup>2,3</sup>, Traver Hart<sup>2,8</sup>, Xiaowei Wang<sup>2,4</sup>, Xiaoyu Zhang<sup>2,3</sup>, Mélanie Robitaille<sup>1</sup>, Kevin R Brown<sup>2</sup>, Sridevi Jaksani<sup>5</sup>, René Overmeer<sup>5</sup>, Sylvia F Boj<sup>5</sup>, Jarrett Adams<sup>2</sup>, James Pan<sup>2,4</sup>, Hans Clevers<sup>5</sup>, Sachdev Sidhu<sup>2,3,6</sup>, Jason Moffat<sup>2,3,6</sup> & Stéphane Angers<sup>1,7</sup>

**Forward genetic screens with CRISPR–Cas9 genome editing enable high-resolution detection of genetic vulnerabilities in cancer cells.** We conducted genome-wide CRISPR–Cas9 screens in *RNF43*-mutant pancreatic ductal adenocarcinoma (PDAC) cells, which rely on Wnt signaling for proliferation. Through these screens, we discovered a unique requirement for a Wnt signaling circuit: engaging FZD5, one of the ten Frizzled receptors encoded in the human genome. Our results uncover an underappreciated level of context-dependent specificity at the Wnt receptor level. We further derived a panel of recombinant antibodies that reports the expression of nine FZD proteins and confirms that *FZD5* functional specificity cannot be explained by protein expression patterns. Additionally, antibodies that specifically bind FZD5 and FZD8 robustly inhibited the growth of *RNF43*-mutant PDAC cells grown *in vitro* and as xenografts *in vivo*, providing orthogonal support for the functional specificity observed genetically. Proliferation of a patient-derived PDAC cell line harboring an *RNF43* variant was also selectively inhibited by the FZD5 antibodies, further demonstrating their use as a potential targeted therapy. Tumor organoid cultures from colorectal carcinoma patients that carried *RNF43* mutations were also sensitive to the FZD5 antibodies, highlighting the potential generalizability of these findings beyond PDAC. Our results show that CRISPR-based genetic screens can be leveraged to identify and validate cell surface targets for antibody development and therapy.

In multicellular organisms, Wnt signaling pathways influence proliferation and differentiation of stem and progenitor cells during embryonic development and adult tissue homeostasis<sup>1,2</sup>. Deregulation of Wnt–β-catenin signaling has been linked to tumor initiation and maintenance in several human malignancies<sup>3</sup>. In most tumors, Wnt–β-catenin signaling is increased as a result of either inactivating mutations in genes encoding proteins that negatively regulate this signaling pathway, such as adenomatous polyposis coli (*APC*) and axin (*AXIN1*) or activating mutations in the gene encoding β-catenin (*CTNNB1*)<sup>4</sup>. In these cases, the signaling pathway is activated distally from the Wnt receptor complex at the cell surface. This complex is composed of one of the ten Frizzled (FZD) proteins and one of the two co-receptor low-density lipoprotein receptor-related proteins, either LRP5 or LRP6 (LRP5/6); thus, developing drugs designed to inhibit the Wnt pathway has proven challenging<sup>5</sup>.

Recent next-generation sequencing studies of gastric, ovarian and pancreatic neoplasias, in addition to colorectal adenocarcinoma and endometrial carcinoma, have identified recurrent non-synonymous *RNF43* mutations<sup>6–11</sup> that appear to be mutually exclusive with *APC*

and *CTNNB1* mutations. *RNF43* and its homolog *ZNRF3* encode transmembrane E3 ubiquitin ligases that target FZD receptors; thus, loss-of-function mutations of either gene lead to high FZD expression at the cell surface and render tumor cells dependent on Wnt ligands for their survival and proliferation<sup>11,12</sup>. Epithelial organoids derived from tumors isolated from *RNF43*<sup>−/−</sup>; *ZNRF3*<sup>−/−</sup> mice grow in the absence of the Wnt amplifier R-spondins, which are secreted proteins that downregulate these E3 ligases<sup>12</sup>—a response that highlights their hypersensitivity to Wnt<sup>11</sup>. Importantly, the growth of these organoids is blocked by inhibition of porcupine (PORCN), an O-acyltransferase required for the maturation and activity of Wnt proteins, which indicates a requirement for Wnt ligands<sup>13</sup>. Treatment of *RNF43*<sup>−/−</sup>; *ZNRF3*<sup>−/−</sup> mutant mice with a PORCN inhibitor represses the growth of intestinal tumors while leaving adjacent normal crypt intact, revealing that a therapeutic window exists to block overactive Wnt pathway activity upstream of β-catenin in *RNF43*- or *ZNRF3*-mutant cancers<sup>13</sup>. Furthermore, screening the sensitivity of 39 human pancreatic ductal adenocarcinoma (PDAC) cell lines to the PORCN inhibitor LGK974 revealed three lines to be highly sensitive

<sup>1</sup>Department of Pharmaceutical Sciences, Leslie Dan Faculty of Pharmacy, University of Toronto, Toronto, Ontario, Canada. <sup>2</sup>Donnelly Centre, University of Toronto, Toronto, Ontario, Canada. <sup>3</sup>Department of Molecular Genetics, University of Toronto, Toronto, Ontario, Canada. <sup>4</sup>The Centre for the Commercialization of Antibodies and Biologics, Toronto, Ontario, Canada. <sup>5</sup>Hubrecht Institute for Developmental Biology and Stem Cell Research, University Medical Centre, Utrecht, Foundation, Hubrecht Organoid Technology, Utrecht, the Netherlands. <sup>6</sup>Canadian Institute for Advanced Research, Toronto, Ontario, Canada. <sup>7</sup>Department of Biochemistry, University of Toronto, Toronto, Ontario, Canada. <sup>8</sup>Present address: Department of Bioinformatics and Computational Biology, University of Texas MD Anderson Cancer Center, Houston, Texas, USA (T.H.). Correspondence should be addressed to S.A. (stephane.angers@utoronto.ca), J.M. (j.moffat@utoronto.ca) or S.S. (sachdev.sidhu@utoronto.ca).

Received 8 August; accepted 30 September; published online 21 November 2016; corrected after print 20 September 2017; doi:10.1038/nm.4219

in clonogenic growth assays, suggesting that a subset of pancreatic tumors depend on Wnt signaling<sup>14</sup>. Each of these cell lines was found to have homozygous loss-of-function *RNF43* mutations, signifying that *RNF43* mutant status could act as a biomarker to predict response to Wnt signaling inhibitors.

The CRISPR–Cas9 system has enabled simple, efficient genome editing and has unlocked the power of genetic screens in human cells<sup>15</sup>. We and other researchers have developed lentiviral-based pooled guide RNA (gRNA) libraries to perform genetic screens to identify fitness genes in human cell lines<sup>16–19</sup>. This work uncovered ~2,000 essential genes in each cell line, including a common core of ~1,600 essential genes<sup>16,18</sup>. ~400 genotype-specific or context-dependent fitness genes were also identified for each of the cell lines studied, exposing vulnerabilities that may be tractable therapeutic targets<sup>16,18</sup>. Because of the urgent need for new therapeutic strategies for pancreatic cancer, we applied genome-scale pooled CRISPR screening technology to identify vulnerabilities in *RNF43*-mutant pancreatic adenocarcinomas and identified the Wnt receptor Frizzled-5 (FZD5) as a common vulnerability that can be exploited therapeutically with antagonistic antibodies.

## RESULTS

### CRISPR–Cas9 screen for vulnerabilities of *RNF43*-mutant PDAC cells

To identify context-dependent fitness genes in *RNF43*-mutant pancreatic cancer cells, we first carried out a genome-wide screen using the HPAF-II human PDAC cell line that is sensitive to PORCN inhibition<sup>14</sup>. Prior to performing this screen, we validated *RNF43* mutation status. We then generated clonal cells expressing *Streptococcus pyogenes* Cas9 (HPAF-II–Cas9) using lentivirus and validated their sensitivity to the PORCN inhibitor LGK974 (Supplementary Fig. 1a–c). A forward genetic screen was carried out in HPAF-II–Cas9 cells using the TKO gRNA library<sup>16</sup>, which contains 91,320 gRNAs targeting 17,232 human genes. This screen was performed in order to identify the set of fitness genes required for the proliferation of these cells. Following infection of HPAF-II–Cas9 cells with the TKO gRNA library, we monitored evolving cell populations over ~20 doublings by deep sequencing of gRNAs (Supplementary Table 1). The fold-change distribution of gRNAs targeting essential genes was significantly shifted relative to those targeting nonessential genes; this shift increased with time, indicating that the screens functioned as designed (Fig. 1a). We then used the BAGEL algorithm<sup>16,20</sup> to calculate a log Bayes factor (BF) for each gene (Supplementary Table 2). BF is a measure of the confidence that knockout of a specific gene causes a decrease in fitness (high BF indicates increased confidence that the knockout of the gene results in a decrease in fitness). Empirically determined reference sets of essential and nonessential genes<sup>21</sup> were used to calculate precision and recall plots (Supplementary Fig. 2a). A total of 2,174 fitness genes were identified in HPAF-II cells (false discovery rate (FDR) < 5%), including 1,315 of 1,580 (83%) previously identified core fitness genes<sup>16</sup>. As expected, several genes encoding core components of the Wnt pathway, including *WLS*, *CTNNB1*, *TCF7L2*, *LRP5* and *PORCN*, were essential in HPAF-II cells. Surprisingly, out of the 10 Frizzled (FZD) receptors and 19 Wnts encoded in the human genome, only 3 genes were essential: *FZD5*, *WNT7B* and *WNT10A* (Fig. 1b). In contrast, genes encoding core negative regulators of the Wnt–β-catenin pathway, including *APC*, *GSK3B* and *ZNRF3*, were found amongst the lowest BF scores, suggesting that knockout of these genes provides a proliferation advantage to HPAF-II cells (Fig. 1b). Based on the list of genes identified in this screen, we generated

a schematic of the proteins involved in Wnt–β-catenin signal transduction in HPAF-II PDAC cells (Fig. 1c).

To determine if these findings are specific to the HPAF-II PDAC cell line, we performed genome-wide fitness screens in two additional *RNF43*-mutant human PDAC lines, AsPC-1 and PaTu8988S (Supplementary Fig. 1d–i, Supplementary Table 1). Both screens exhibited substantial shifts in the distribution of reference essential genes in comparison to nonessential genes (Supplementary Fig. 2b,c). These screens identified 936 and 2,071 fitness genes (FDR < 5%), respectively (Supplementary Table 2), which included genes encoding several members of the Wnt pathway (Fig. 1e, Supplementary Fig. 2d,e).

We next examined the context-dependent fitness genes that were specific to *RNF43*-mutant PDAC cells in comparison to other non-PDAC cell lines, which are wild type for *RNF43* and were previously screened with the TKO library<sup>16</sup>. For each gene, we calculated the difference between average normalized BF scores observed in *RNF43*-mutant PDAC cell lines and the average BF scores across the five previously reported screens (HCT116, DLD-1, RPE1, GBM, HeLa). That difference was then converted to a z-score (Supplementary Table 3). The fitness gene profile of HPAF-II and PaTu8988S (*RNF43* mutant) was most similar to those of DLD-1 and HCT116 colorectal cancer cells (Supplementary Fig. 2f), which may reflect the common endodermal origin of these cell lines. Examination of the top differential fitness genes readily highlighted the known addiction of these PDAC cells to Wnt–β-catenin signaling, since we observed several genes previously encoding proteins described as positive regulators of this pathway having z-scores of  $\geq 2$  (*FZD5*, *WLS*, *PORCN*, *WNT3*, *TCF7L2*, *CTNNB1* (β-catenin), *LRP6*, *LRP5*, *WNT7B*) (Fig. 1d). We next compared high-confidence essential genes from our screens in *RNF43*-mutant PDAC cells with a panel of recently published and high-quality (according to the BAGEL pipeline and excluding L3.3 cells, Supplementary Fig. 2g) CRISPR–Cas9 screens in seven additional PDAC cell lines<sup>22</sup>, which are all insensitive to PORCN inhibitors<sup>14</sup>. These analyses revealed that *RNF43*-mutant PDAC cells selectively depend on Wnt–β-catenin signaling for their proliferation and/or survival and exclude the possibility that these genes are merely lineage-specific fitness genes (Fig. 1e). Intriguingly, of the ten FZD genes encoded in the human genome, only *FZD5* was essential in *RNF43*-mutant PDAC cells.

### *FZD5* is required for the growth of *RNF43*-mutant PDAC cells

To validate the screen results we infected human PDAC *RNF43*-mutant HPAF-II–Cas9 cells with individual lentivirus expressing targeting gRNAs. We then performed clonogenic growth assays. Knockout of *FZD5* using two individual gRNAs selected from the TKO library led to robust growth inhibition, comparable to treatment with a gRNA targeting β-catenin or the PORCN inhibitor LGK974 (Fig. 2a). In contrast, cells transduced with a control *LacZ* gRNA or two unique and validated gRNAs for each of *FZD4*, *FZD7* or *FZD8* (Fig. 2b, Supplementary Fig. 11a and Supplementary Table 4) exhibited normal growth (Fig. 2a). We also tested whether *FZD5* was required specifically for the growth of the other *RNF43*-mutant PDAC cell lines. Results indicated that *FZD5* gRNAs, but not *FZD7* gRNAs, inhibited the growth of HPAF-II, PaTu8988S and AsPC-1 cells to levels similar to those in cells treated with LGK974 or transduced with the *CTNNB1* gRNA (Fig. 2c). In contrast, the growth of the PANC-1, BxPC-3 and YAPC PDAC cell lines, which are insensitive to LGK974 (ref. 14), was not inhibited by gRNAs targeting *FZD5*, *FZD7* or *CTNNB1* (Fig. 2c). The editing efficiency of each gRNA

targeting *FZD5* or *FZD7* was quantified using Tracking of Indels by DEcomposition (TIDE)<sup>23</sup> (**Supplementary Fig. 3a–c**) or confirmed with a T7 endonuclease I assay (**Supplementary Figs. 3d** and **11b**). Editing of *FZD5* led to marked inhibition of expression of the Wnt target genes *AXIN2* and *NKD1*, which is consistent with aforementioned

results and provides support for a key role of *FZD5* in transducing autocrine Wnt– $\beta$ -catenin signaling in *RNF43*-mutant cells. Minimal or no change was observed in cells transduced with *FZD7* gRNAs (**Fig. 2d,e**). Furthermore, knocking out *FZD5* or *CTNNB1*, or treating cells with LGK974, led to increased expression of the differentiation

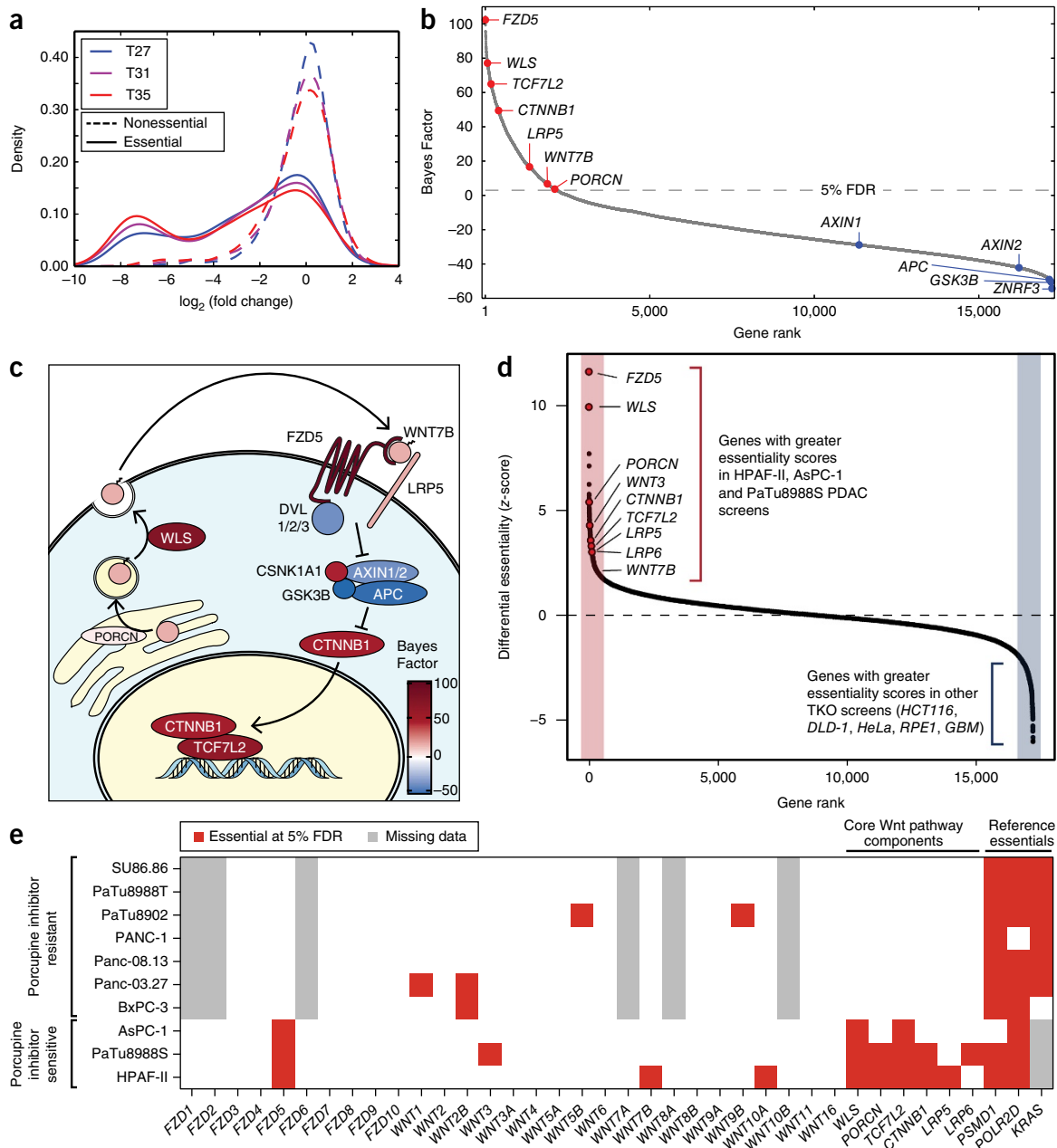


**Figure 1** Genome-wide CRISPR–Cas9 screens identify genetic vulnerabilities of *RNF43*-mutant PDAC cells. **(a)** Fold change distributions of gRNA targeting essential genes (solid lines) or nonessential genes (dashed lines) at the indicated time points (27, 31 and 35 d) after infection of HPAF-II cells with the TKO gRNA library. **(b)** Ranked gene-level fitness scores (Bayes factors) from genome-wide CRISPR fitness screen in HPAF-II cells. Selected genes with known function in Wnt signaling are indicated. **(c)** Schematic of factors implicated as essential for Wnt signal transduction in HPAF-II in the CRISPR–Cas9 screen. In this proposal, autocrine WNT7B binds to the FZD5–LRP5 receptor complex, which through the action of DVL1, DVL2 and DVL3 (all three nonessential), inhibits the destruction complex, composed of AXIN1, AXIN2, APC, GSK3B and CSNK1A1. This allows for relief on inhibition on  $\beta$ -catenin (CTNNB1), which can now translocate to the nucleus and activate the TCF7L2 transcription factor. Each protein is shaded according to its BF or average BF when multiple isoforms are present (for example, DVL1, DVL2 and DVL3, and AXIN1 and AXIN2). **(d)** Ranked differential fitness score reveals context dependent vulnerabilities in PDAC cells. Mean BF from PDAC screens were compared to mean BF from HeLa, HCT116, DLD-1, RPE-1 and GBM and converted to a z-score. **(e)** High-confidence Wnt pathway essential genes identified across various PDAC cell lines using CRISPR screens (this study and ref. 22). Three PORCN inhibitor sensitive lines that are *RNF43*-mutant (HPAF-II, AsPC-1 and PaTu8988S) and seven PORCN inhibitor resistant cell lines (indicated) are compared.

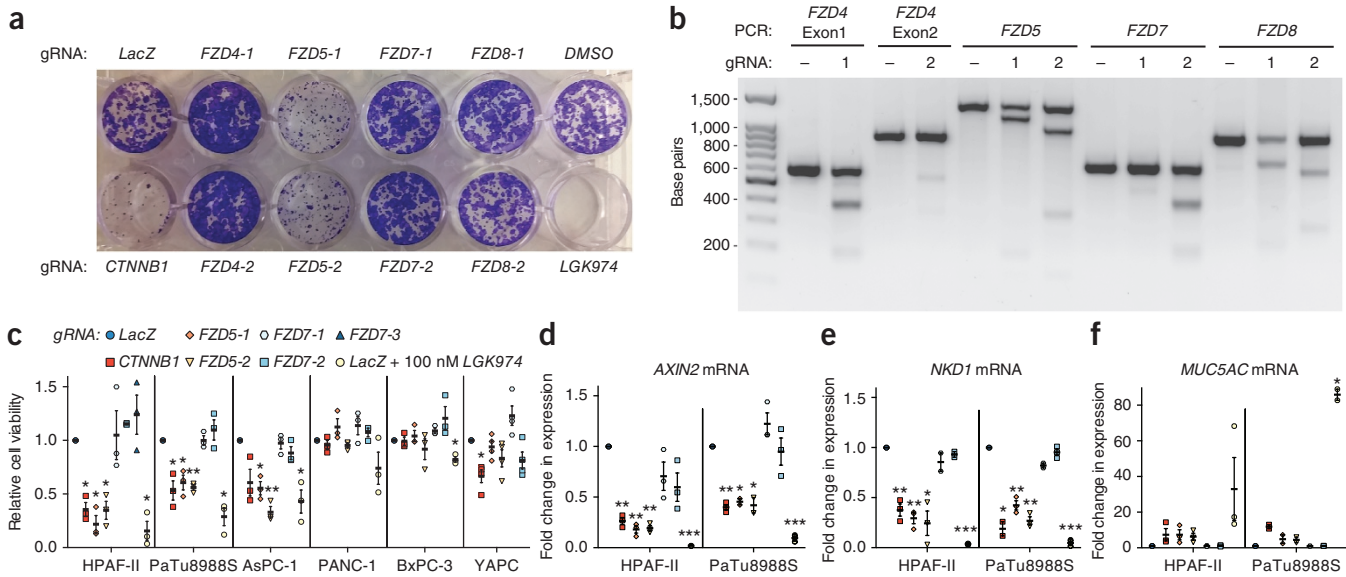


**Figure 2** FZD5 knockout inhibits proliferation of *RNF43*-mutant PDAC cell lines and Wnt target genes activation. **(a)** Clonogenic proliferation assay in HPAF-II cells stably expressing Cas9 and transduced with lentivirus delivering indicated gRNA. Representative of three independent experiments. **(b)** T7 endonuclease I cleavage assay confirms gRNA-mediated gene editing in transduced HPAF-II-Cas9 cells. Expected digest products are located in **Supplementary Table 4**. Representative of three independent experiments. **(c)** Cell viability assays in various PDAC cell lines stably expressing Cas9 (polyclonal), transduced with lentivirus delivering indicated gRNAs. HPAF-II, PaTu8988S and AsPC-1 are sensitive to Wnt pathway inhibition and contain *RNF43* mutations. PANC-1, BxPC-3 and YAPC are insensitive to Wnt pathway inhibition. **(d–f)** RT-qPCR of Wnt target genes (*AXIN2*, *NKD1*) and differentiation induced gene, *MUC5AC* ( $n = 2$  independent experiments for PaTu8988S), in HPAF-II and PaTu8988S Cas9 cell lines transduced with lentivirus delivering indicated gRNA. All dots represent mean of an independent experiment, performed in technical triplicate. All bars represent mean  $\pm$  s.e.m.,  $n = 3$  independent experiments unless otherwise noted. \*\*\* $P < 0.001$ , \*\* $P < 0.01$ , and \* $P < 0.05$ , one-sample *t*-test.

marker *MUC5AC*<sup>14</sup>, whereas no change was observed in *RNF43*-mutant PDAC cells knocked out for FZD7 (Fig. 2f). We conclude that FZD5 is essential for the proliferation of *RNF43*-mutant PDAC cells.

#### FZD5 dependency is not explained by cell-specific mRNA or protein expression

Given the potential combinatorial complexity of the Wnt pathway (i.e., 19 Wnts and 10 FZDs), we were surprised to find that a single FZD homolog, FZD5, is required to drive cellular proliferation in HPAF-II, PaTu8988S and AsPC-1 cells. Furthermore, only one or two genes encoding Wnt ligands were identified as essential in each *RNF43*-mutant PDAC cell line (Fig. 1e). RNA-seq analysis revealed that several of the Wnt genes and FZD genes are expressed in these cells, which suggests that their specific dependence on the FZD5 circuit is likely not due to lack of expression of other FZD proteins (Fig. 3a). To examine the possibility of a disconnect between RNA and the protein levels for the FZD receptors in PDAC cell lines, we generated a panel of recombinant antibodies which can detect and discriminate all but one of the ten FZD receptors. Briefly, we used a phage-displayed fragment antigen-binding (Fab) library<sup>24</sup> and performed binding selections on the purified cysteine-rich domains (FZD-CRDs) (Supplementary Fig. 4a) of each of the ten human FZD proteins except FZD3, which we could not purify (Fig. 3b). We chose the most selective Fabs for each of the FZD-CRDs based on phage-Fab ELISAs and converted these to purified Fabs. To characterize the binding specificity of the Fabs on cells, we generated a panel of ten CHO cell lines, each expressing the CRD domain of a different myc-tagged FZD receptor anchored at the plasma membrane through a GPI anchor (CHO-myc-FZD-GPI). Despite the high sequence identity between Frizzled family members (Supplementary Fig. 4b-d),

we were able to identify selective Fabs for FZD4, FZD5, FZD6 and FZD10 as assessed by flow cytometry (Fig. 3c, Supplementary Fig. 5). Moreover, we found Fabs that bound to FZD1 and FZD7 (hereafter FZD1/7), FZD2/7, FZD5/8, FZD1/2/5/7/8 or FZD4/9/10, which can be used to discriminate expression of the remaining FZDs excluding FZD3 (Fig. 3c, Supplementary Fig. 5). The ‘FZD profiler’ therefore consists of ten different Fabs that can be used to discriminate expression of different FZD homologs. The FZD profiler was then used to confirm that HPAF-II cells express, at minimum, FZD1, FZD5 and FZD6, and possibly FZD8, at the cell surface (Fig. 3d,e).

Since multiple FZD receptors are expressed at the surface of HPAF-II cells, we predicted that stimulation of these receptors with high levels of exogenous Wnt3A would bypass the ligand-receptor pair specificity, and this could rescue the growth inhibition imparted by *WNT7B* or FZD5 knockout in HPAF-II cells. Treatment of FZD5 or *WNT7B* (but not *CTNNB1*) knockout cells with Wnt3A-conditioned medium (CM) rescued their growth (Fig. 3f), as well as the expression of the Wnt target genes *AXIN2* and *NKD1* (Fig. 3g,h), confirming this prediction. We conclude that at endogenous levels of Wnt ligands, FZD5 acts as the chief receptor to transduce Wnt-β-catenin signaling in the context of *RNF43*-mutant PDAC cells.

#### Anti-FZD5 antibodies inhibit the growth of *RNF43*-mutant PDAC

Based on our results showing that FZD5 is the FZD receptor essential for the growth of *RNF43*-mutant PDAC cells, we next developed anti-FZD5 full-length human recombinant antibodies and evaluated both their binding properties and efficacy in *RNF43*-mutant PDAC cells. Using the antibody phage-display system described above and selecting on purified FZD5-CRD, we isolated two Fabs (Fab-2919 and Fab-2921) that exhibited high-affinity binding to human FZD5-CRD but also exhibited some cross reactivity to FZD8-CRD

(Supplementary Fig. 5). We then converted these Fabs to full-length IgG1 proteins (IgG-2919 and IgG-2921) and tested whether these IgGs inhibited the proliferation of *RNF43*-mutant PDAC cells. IgG-2919 and IgG-2921 were compared directly with OMP-18R5, a

FZD7-derived antibody currently in clinical trials, which shows cross reactivity to FZD1, FZD2, FZD5, FZD7 and FZD8 (ref. 25). Treatment of *RNF43*-mutant PDAC cell lines HPAF-II, PaTu8988S and AsPC-1 with the FZD5 IgGs led to dose-dependent anti-proliferative effects,

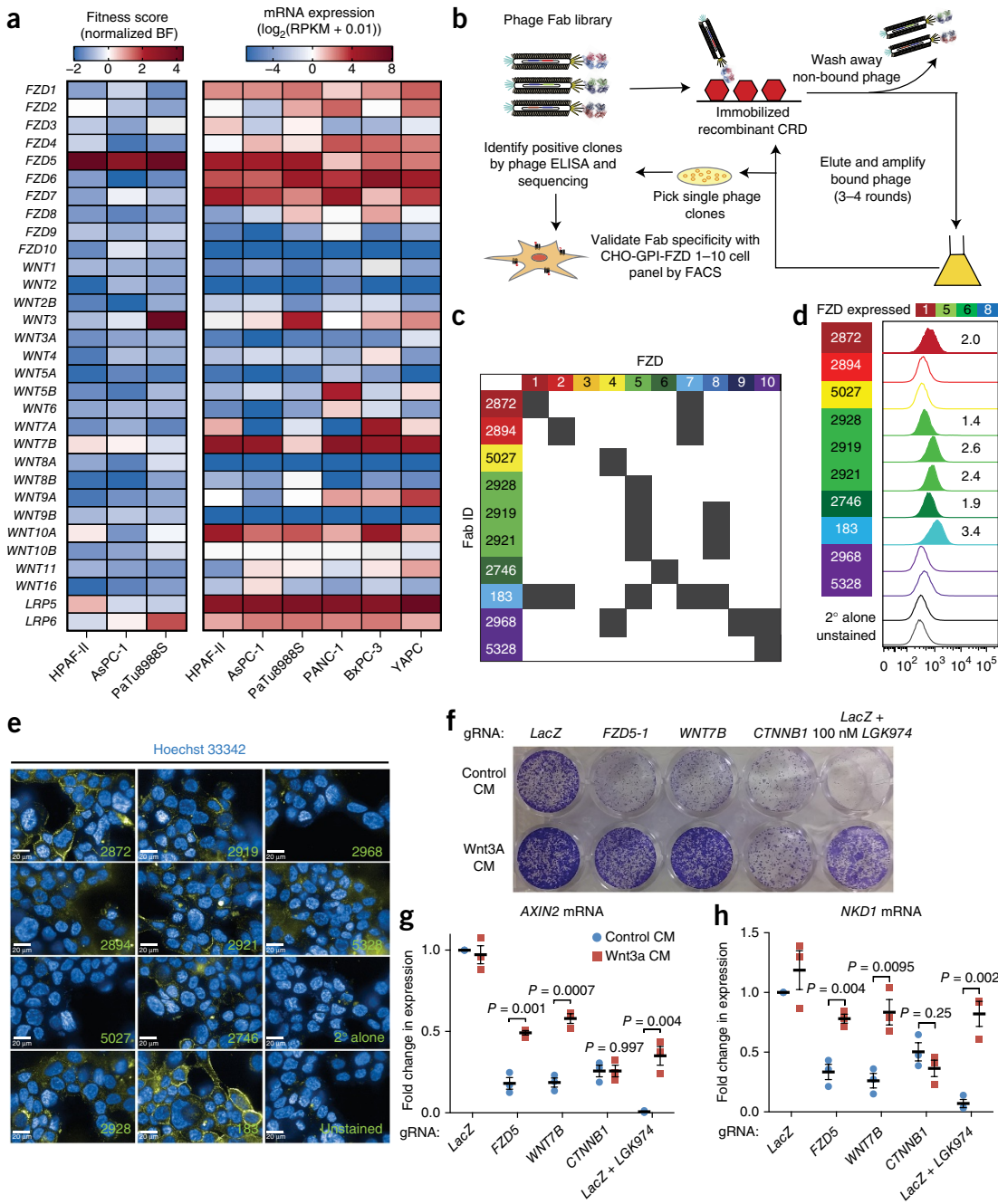


**Figure 3** Wnt and Frizzled expression patterns are not predictive of essentiality. (a) z-score-normalized BF and mRNA expression for all *FZD* receptor, *WNT* ligand and *LRP5* and *LRP6* co-receptor genes in indicated PDAC cell lines. (b) Schematic for Fab selection by phage display. (c) Specificity profile of anti-FZD Fabs forming the ‘FZD profiler’, as determined by flow cytometry in FZD-CRD-overexpressing CHO cell lines (Supplementary Fig. 5). Color of each ID box corresponds to the color of the purified FZD CRD used to isolate the Fab in selections. (d) Determination of FZD receptor membrane expression in HPAF-II cells. Values indicate median fluorescence intensity (MFI). MFI greater than 1.35 $\times$  that for the secondary antibody alone was taken as evidence of endogenous expression and histograms were filled in this case. This figure is representative of, at minimum, 10,000 cells per sample in a single experiment. FZD receptors determined to be found at the surface of HPAF-II are indicated above. (e) Indirect immunofluorescence, using the different anti-Frizzled Fabs, showing cell surface expression in HPAF-II cells. Images are representative of at minimum 15 images from one experiment performed in technical duplicate. Scale bars, 20  $\mu$ m. (f) Wnt3A conditioned media (CM) rescues proliferation defect (representative of 4 independent experiments) and (g,h) Wnt target gene expression in *FZD5*- and *WNT7B*- but not in *CTNNB1*-knockout HPAF-II cells. Each dot represents mean of one independent experiment performed in technical triplicate. Bars represent mean  $\pm$  s.e.m.,  $n = 3$  independent experiments. Two-tailed unpaired t-test.

whereas OMP-18R5 had some effects on AsPC-1 cellular proliferation at high doses but no significant effects on HPAF-II or PaTu8988S proliferation at the doses tested (Fig. 4a–c). Additionally, the FZD5 IgGs

had negligible or no effect in the *RNF43* wild-type PANC-1, BxPC-3 or YAPC cells (Fig. 4d–f). When we examined the binding of the FZD5 Fabs to these cell lines via immunofluorescence, we consistently

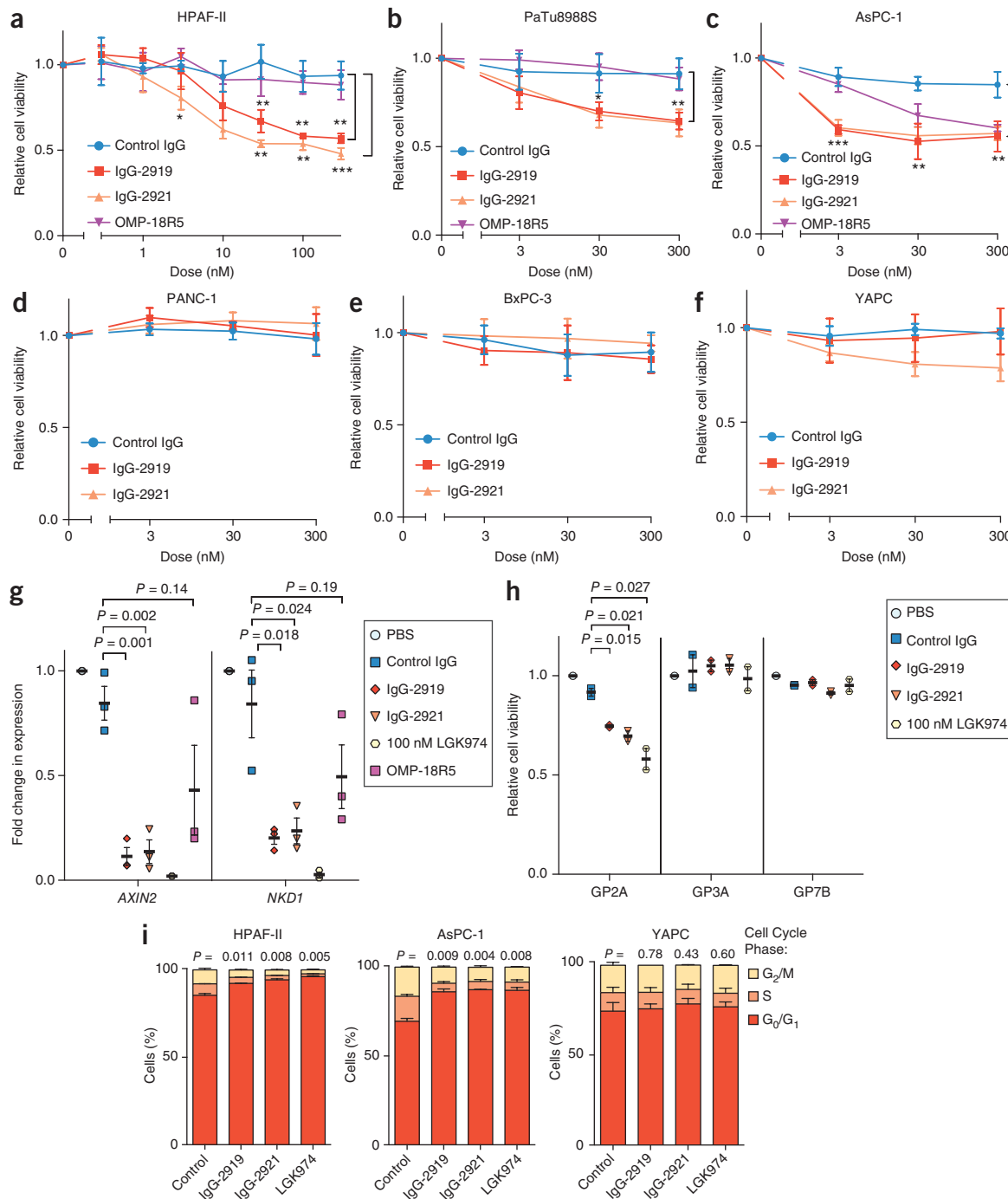


**Figure 4** Anti-FZD5 antibodies inhibit growth of *RNF43*-mutant PDAC through cell-cycle arrest. **(a–f)** Cell viability assays in *RNF43*-mutant and Wnt dependent cell lines (HPAF-II, AsPC-1 and PaTu8988S) and Wnt insensitive cell lines (PANC-1, BxPC-3 and YAPC). Cells were treated with indicated doses of IgG-2919, IgG-2921 or OMP-18R5. Points represent mean  $\pm$  s.d.,  $n = 3$  independent experiments. \*\*\* $P < 0.001$ , \*\* $P < 0.01$ , and \* $P < 0.05$ , two-tailed unpaired *t*-test. **(g)** RT-qPCR of Wnt- $\beta$ -catenin target genes *AXIN2* and *NKD1* in HPAF-II after treatment with 300 nM IgG-2919, IgG-2921, OMP-18R5 or 100 nM of the PORCN inhibitor LGK974. Dots represent mean of one independent experiment performed in technical triplicate. Bars represent mean  $\pm$  s.e.m.,  $n = 3$  independent experiments. Two-tailed unpaired *t*-test. **(h)** Cell viability assays in three PDAC patient-derived cell lines, each treated with 300 nM IgG-2919, IgG-2921 or 100 nM LGK974. GP2A contains a homozygous *RNF43* variant, whereas GP3A and GP7A are *RNF43* WT. Each dot represents mean of one independent experiment performed in technical triplicate. Bars represent mean  $\pm$  s.e.m.,  $n = 2$  independent experiments. Two-tailed unpaired *t*-test. **(i)** DNA-content staining based cell-cycle analysis in HPAF-II, AsPC-1 and YAPC, treated with PBS control, IgG-2919, IgG-2921 or LGK974 (200 nM each). Bars represent mean  $\pm$  s.d.,  $n = 2$  independent experiments, all statistical tests based on proportion of cells in G<sub>0</sub>/G<sub>1</sub>, compared to control. Two-tailed unpaired *t*-test.

found clear binding to the sensitive cell lines, but we detected little to no binding in resistant lines, indicating possible overexpression of FZD5 at the protein level. (Supplementary Fig. 6). Notably, anti-FZD5 IgG treatment, in comparison to control IgG treatment, led to inhibition of *AXIN2* and *NKD1* mRNA; this demonstrates specific Wnt–β-catenin pathway inhibition (Fig. 4g). Addition of exogenous Wnt3A-CM was able to rescue the growth of IgG-2919 treated cells (Supplementary Fig. 7a). Taken together, these results demonstrate that anti-FZD5 IgGs mimic the genetic knockout of FZD5 and inhibit the proliferation of *RNF43*-mutant PDAC cells *in vitro*.

To further explore the utility of using IgG-2919 or IgG-2921 in more representative PDAC tumor models, we tested the effects of IgG-2919 and IgG-2921 in three individual patient-derived PDAC early-passage cell lines and observed significant anti-proliferative efficacy in GP2A cells (Fig. 4h). GP2A cells harbor an *RNF43*

variant (R117H) (Supplementary Fig. 8) previously linked to PDAC in a genome-wide association study<sup>26</sup> and shown to affect *RNF43* mRNA stability<sup>27</sup>. Treatment of GP3A or GP7B cells, which are wild type for *RNF43*, with IgG-2919 or IgG-2921 had no effects on cell proliferation (Fig. 4h).

We were also interested in whether the decrease in cells' viability by the anti-FZD5 IgGs was a result of cytostasis and/or cytotoxicity. DNA content staining, followed by flow cytometry, revealed cell cycle arrest in the G<sub>0</sub>/G<sub>1</sub> cell-cycle phase. Treatment with IgG-2919, IgG-2921 or LGK974 in HPAF-II and AsPC-1 caused a significant increase in the percentage of cells in G<sub>0</sub>/G<sub>1</sub> and decrease in S, G<sub>2</sub> or M phase (Fig. 4i, Supplementary Fig. 7b). Conversely, no change was detected in LGK974-insensitive YAPC cells. Finally, treatment of HPAF-II cells with IgG-2919 induced no detectable caspase-3 cleavage, suggesting that inhibition of Wnt signaling does not lead to apoptosis in this context (Supplementary Figs. 7c and 11c). We conclude that FZD5

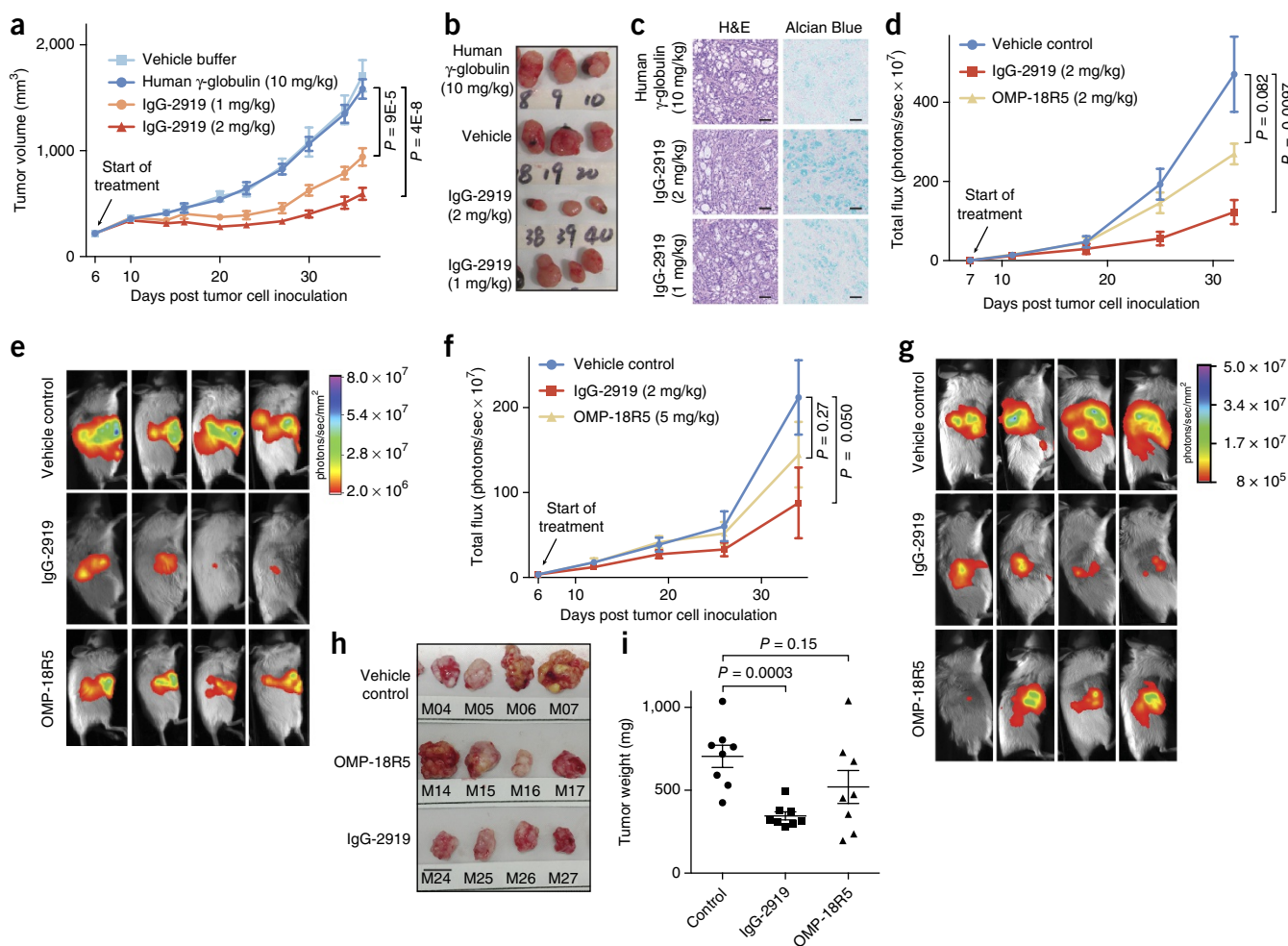


**Figure 5** Anti-FZD5 antibodies inhibit growth of *RNF43*-mutant PDAC in *in vivo* xenograft models. (a) HPAF-II cells were grown as subcutaneous xenografts, and when tumors reached 200 mm<sup>3</sup>, mice were divided into groups and dosed intraperitoneally ( $n = 9$  for vehicle and 1 mg/kg IgG-2919 conditions,  $n = 10$  for human γ-globulin and 2 mg/kg IgG-2919 conditions). (b) Representative images of xenograft tumors obtained in a. (c) Histological staining of representative tumors from control and antibody-treated xenograft models. Scale bars, 100 μm. (d) Luciferase-expressing HPAF-II cells were grown as orthotopic xenografts and dosed with PBS vehicle control, 2 mg/kg IgG-2919 or 2 mg/kg OMP-18R5. Tumor size was measured by quantification of photon flux.  $n = 8$  for each condition, except vehicle control day 32 ( $n = 7$ ). (e) Representative bioluminescence images obtained at day 32 in d. (f) Luciferase-expressing AsPC-1 cells were grown as orthotopic xenografts and dosed with PBS vehicle control, 2 mg/kg IgG-2919 or 5 mg/kg OMP-18R5. Tumor size was measured by quantification of photon flux.  $n = 9$  per group. (g) Representative bioluminescence images obtained at day 34 in f. (h) Representative images of AsPC-1 tumors dissected at 37 d post inoculation. Scale bar, 1 cm. (i) Weights of AsPC-1 tumors after dissection ( $n = 8$ ). All data are represented as mean ± s.e.m., two-tailed unpaired t-test.

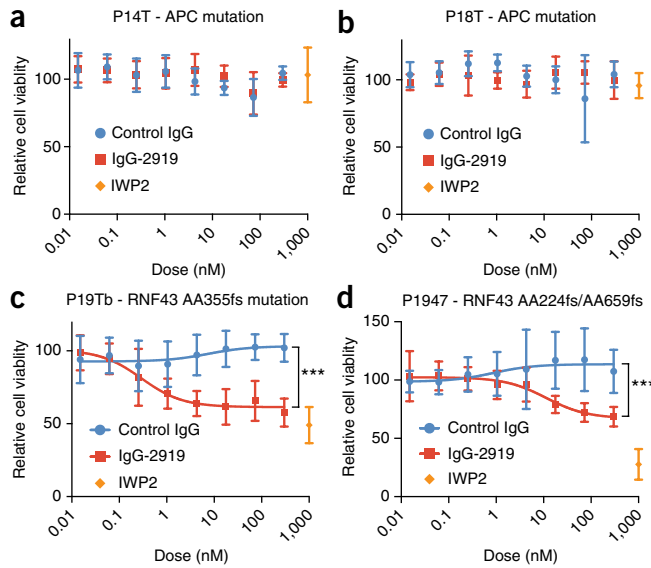


**Figure 6** Anti-FZD5 IgG inhibits survival of *RNF43*-mutant colorectal cancer (CRC) organoids. **(a–d)** Cell viability assays for two APC-mutant (**a,b**) and two *RNF43*-mutant (**c,d**) CRC-patient-derived organoid lines when treated with various doses of anti-FZD IgG-2919 or with a maximal dose of the PORCN inhibitor IWP2. Data were fitted using nonlinear regression.  $n = 2$  independent experiments run in technical triplicates. \*\*\* $P < 0.001$ , extra sum of squares F-test.

antibodies inhibit the proliferation of *RNF43*-mutant PDAC cells in culture through G<sub>0</sub>/G<sub>1</sub> cell-cycle arrest.

We next evaluated the effect of IgG-2919 on tumor growth *in vivo* in immunodeficient mice bearing subcutaneous HPAF-II xenografts. Treatment with 1 or 2 mg/kg IgG-2919 at 200 mm<sup>3</sup> tumor size led to 46% or 73% tumor growth inhibition, respectively (Fig. 5a,b and Supplementary Fig. 9a,b). There were no changes in body weight or visual signs of toxicity (Supplementary Fig. 9c). Histological analysis of the tumors revealed increased mucin production, as visualized by PAS and Alcian Blue staining, consistent with cellular differentiation (Fig. 5c, Supplementary Fig. 9d)<sup>14</sup>. Since the residual tumors are filled with mucin, it is important to note that the efficacy of the antibodies may be underestimated.

To further explore the therapeutic potential of targeting *RNF43*-mutant PDAC tumors with anti-FZD5 antibodies, we established orthotopic pancreatic tumors in mice with luciferase-expressing HPAF-II or AsPC-1 cells. We then monitored tumor growth in live animals using bioluminescence imaging and initiated therapeutic treatments twice a week with either IgG-2919 or OMP-18R5 starting 6 (AsPC-1 model) or 7 d (HPAF-II model) after tumor cell inoculation. In HPAF-II orthotopic tumors treated with 2 mg/kg IgG-2919 or OMP-18R5, we observed 74% ( $P = 0.0097$ ) and 42% ( $P = 0.082$ ) growth inhibition, respectively, over a 32-d experiment compared with control tumors (Fig. 5d,e, Supplementary Fig. 10a) with no weight loss (Supplementary Fig. 10b). Similarly, AsPC-1 orthotopic tumors treated with 2 mg/kg IgG-2919 or 5 mg/kg OMP-18R5 led to 60% ( $P = 0.05$ ) and 32% ( $P = 0.27$ ) growth inhibition, respectively, compared with control tumors (Fig. 5f,g, Supplementary Fig. 10c). At the endpoint of the AsPC-1 study, we dissected the tumors from the orthotopic site and weighed them to confirm the growth inhibitory effects of IgG-2919 (51% of control,  $P = 0.0003$ ) (Fig. 5h,i, Supplementary Fig. 10d) with no weight loss (Supplementary Fig. 10e). Thus, although different Wnt ligands are likely present in subcutaneous and orthotopic PDAC tumors, the effects

of the anti-FZD5 antibodies are equally potent in different tumor microenvironments. Taken together, these results indicate that targeting FZD5 with specific antagonistic antibodies represents a new therapeutic opportunity for treatment of *RNF43*-mutant pancreatic cancer.

### Anti-FZD5 antibodies block the growth of *RNF43*-mutant CRC-patient-derived organoids

Given the findings that *RNF43* mutations frequently occur in colorectal cancer (CRC)<sup>9</sup>, we reasoned that FZD5 dependency may also exist in this context. A recent study generated colorectal cancer organoids from 20 patients and examined their sensitivity to a panel of different drugs<sup>28</sup>. Interestingly, one of the tumor organoids (id P19Tb) was found to harbor an *RNF43* mutation and displayed sensitivity to PORCN inhibitors<sup>28</sup>. Therefore, we tested the sensitivity of two patient-derived *RNF43*-mutant CRC organoids and two APC mutant CRC organoids, which are predicted to be insensitive due to distal activation of β-catenin, to IgG-2919 and to the PORCN inhibitor IWP2. We found that the APC-mutant organoids were insensitive to IgG-2919 and IWP2 (Fig. 6a,b), whereas the *RNF43*-mutant CRC organoids were sensitive to both treatments (Fig. 6c,d). These results indicate that FZD5 dependency may be linked with *RNF43* mutation across multiple cancer types, broadening the potential utility of anti-FZD5 antibodies as a targeted cancer therapy.

### DISCUSSION

Our results, which integrated genome-wide screens performed in three independent *RNF43*-mutant PDAC cell lines, identified FZD5 as the only FZD receptor encoded in the human genome as essential for cellular proliferation and solely responsible for transducing the bulk of Wnt-β-catenin signaling in this context. Similarly, a limited selection of Wnt ligands was found to be essential in the different cell lines, with *WNT7B* and *WNT10A* essential in HPAF-II, *WNT7B* in AsPC-1 and *WNT3* in PaTu8988S (Fig. 1e, Supplementary Table 2). *WNT7B* was previously identified as a physiological regulator of pancreatic progenitor cell growth coordinating pancreas development through autocrine signaling in the epithelium and paracrine response in the surrounding mesenchyme<sup>29</sup>. Gene expression analysis and shRNA-mediated knockdown further supported a role for *WNT7B* in PDAC cell growth<sup>30</sup>. *WNT3* mRNA is highly expressed in PaTu8988S cells in comparison with the other PDAC cell lines (Fig. 3a), suggesting the essentiality of Wnt ligands may be governed by expression in some contexts.

Previous attempts at determining whether Wnt ligands exhibit specificity of interaction with the different Frizzled receptors have been largely inconclusive, possibly due to overexpression of proteins not being representative of interactions at endogenous doses<sup>31</sup>. Our study shows that one or two Wnt ligands and only one of the ten FZD receptors are functionally important for proliferation of PDAC cells, despite many Wnts and FZDs being expressed. This indicates that small differences in binding affinities may provide discrimination under normal expression levels. That stimulation with ectopic Wnt3A-CM can rescue the growth of FZD5 or *WNT7B* knockout cells and bypass the endogenous WNT-FZD5 circuit indicates that Frizzled receptors are functional at the surface of these cells and are capable of mounting a β-catenin response. However, FZD5 appears to be the single FZD capable of transducing signals in response to the endogenous doses of Wnts; this suggests the possibility that upregulation of other Wnt ligands beyond a certain threshold could represent a mechanism of resistance to FZD inhibitors.

Unexpectedly, when compared to our anti-FZD5 IgGs as a single-agent therapeutic, OMP-18R5 was less effective in blocking the

growth of *RNF43*-mutant PDAC cells grown *in vitro* or *in vivo* as orthotopic xenografts. Notably, OMP-18R5 reduced Wnt target gene expression but to a lesser degree than IgG-2919 and IgG-2921, suggesting that residual  $\beta$ -catenin signaling may be sufficient to allow for tumor cell proliferation. The molecular basis for the increased efficacies of IgG-2919 and IgG-2921 over OMP-18R5 remain unclear. Differential affinities of binding FZD5 could be one reason, but careful determination of the affinity of the antibodies using surface plasmon resonance did not reveal significant differences (J.A., data not shown). Other potential reasons include the differential ability of the antibodies to compete for Wnt ligand binding, interference with the engagement of the LRP5 or LRP6 co-receptors or negative cooperativity underlying the interaction with FZD5 CRDs. Future work will be needed to better understand the properties of anti-FZD antibodies which are important for maximal therapeutic effect.

Despite the known requirement of the Wnt– $\beta$ -catenin signaling axis in *RNF43*-mutated PDAC<sup>14</sup>, the complexity of this pathway in terms of number of Wnt ligands, FZD receptors and co-receptors and intracellular signaling components makes the prediction of therapeutic targets difficult. The identification of specific genetic vulnerabilities using genome-wide CRISPR-based genetic screens provides an unbiased and powerful means to identify context-specific fitness genes that can be harnessed to treat human diseases such as cancer. Herein we identified FZD5 as the top context-dependent fitness gene in *RNF43*-mutated PDAC and leveraged this finding to guide the development of novel biologics. Our anti-FZD5 antibodies were effective at inhibiting the growth of *RNF43*-mutant PDAC cells in standard cell culture models, patient-derived cells and multiple *in vivo* models, corroborating FZD5 as a therapeutic target in a subset of PDACs. Experiments in CRC organoids also further expand these findings, possibly to other cancers where *RNF43* or *ZNRF3* function is compromised. Moreover, by selectively targeting the exact Wnt signaling circuit activated in various tumors or diseases, FZD-specific antibodies may be less toxic than other approaches that broadly target Wnt signaling.

## METHODS

Methods, including statements of data availability and any associated accession codes and references, are available in the [online version of the paper](#).

*Note:* Any Supplementary Information and Source Data files are available in the [online version of the paper](#).

## ACKNOWLEDGMENTS

We wish to thank members of the Angers and Moffat labs for discussions. We are thankful to D. Hedley (Princess Margaret Hospital, Toronto, Canada) and M. Tsao (Ontario Cancer Institute, Toronto, Canada) for providing the patient-derived xenograft cells; P. Mero (Moffat lab) for help with images. This work was supported from grants funded by the Canadian Institutes for Health Research to S.A. (CIHR-273548) and J.M. (CIHR-342551) and by the Ontario Research Fund to S.S. J.M. holds a Canada Research Chair in Functional Genomics of Cancer and S.A. holds a Canada Research Chair in Functional Architecture of Signal Transduction. Some of the equipment used in this study was supported by The 3D (Diet, Digestive Tract and Disease) Centre funded by the Canadian Foundation for Innovation and Ontario Research Fund, project numbers 19442 and 30961.

## AUTHOR CONTRIBUTIONS

Conceptualization, S.A., J.M., S.S.; investigation, Z.S., Z.P., M.C., T.H., X.W., X.Z., M.R., S.J., R.O., S.E.B., J.A., K.R.B.; writing, S.A., Z.S., J.M.; funding acquisition, S.A., J.M., S.S.; supervision, S.A., J.M., S.S., H.C., and J.P.

## COMPETING FINANCIAL INTERESTS

The authors declare no competing financial interests.

Reprints and permissions information is available online at <http://www.nature.com/reprints/index.html>.

- Wodarz, A. & Nusse, R. Mechanisms of Wnt signaling in development. *Annu. Rev. Cell Dev. Biol.* **14**, 59–88 (1998).
- Schuijers, J. & Clevers, H. Adult mammalian stem cells: the role of Wnt, Lgr5 and R-spondins. *EMBO J.* **31**, 2685–2696 (2012).
- Anastas, J.N. & Moon, R.T. WNT signalling pathways as therapeutic targets in cancer. *Nat. Rev. Cancer* **13**, 11–26 (2013).
- Polakis, P. Wnt signaling in cancer. *Cold Spring Harb. Perspect. Biol.* **4** (2012).
- Madan, B. & Virshup, D.M. Targeting Wnts at the source—new mechanisms, new biomarkers, new drugs. *Mol. Cancer Ther.* **14**, 1087–1094 (2015).
- Waddell, N. *et al.* Whole genomes redefine the mutational landscape of pancreatic cancer. *Nature* **518**, 498–501 (2015).
- Ryland, G.L. *et al.* Mutational landscape of mucinous ovarian carcinoma and its neoplastic precursors. *Genome Med.* **7**, 87 (2015).
- Wang, K. *et al.* Whole-genome sequencing and comprehensive molecular profiling identify new driver mutations in gastric cancer. *Nat. Genet.* **46**, 573–582 (2014).
- Giannakis, M. *et al.* *RNF43* is frequently mutated in colorectal and endometrial cancers. *Nat. Genet.* **46**, 1264–1266 (2014).
- Ivanov, I., Lo, K.C., Hawthorn, L., Cowell, J.K. & Ionov, Y. Identifying candidate colon cancer tumor suppressor genes using inhibition of nonsense-mediated mRNA decay in colon cancer cells. *Oncogene* **26**, 2873–2884 (2007).
- Koo, B.K. *et al.* Tumour suppressor *RNF43* is a stem-cell E3 ligase that induces endocytosis of Wnt receptors. *Nature* **488**, 665–669 (2012).
- Hao, H.X. *et al.* *ZNRF3* promotes Wnt receptor turnover in an R-spondin-sensitive manner. *Nature* **485**, 195–200 (2012).
- Koo, B.K., van Es, J.H., van den Born, M. & Clevers, H. Porcupine inhibitor suppresses paracrine Wnt-driven growth of *Rnf43/Znrf3*-mutant neoplasia. *Proc. Natl. Acad. Sci. USA* **112**, 7548–7550 (2015).
- Jiang, X. *et al.* Inactivating mutations of *RNF43* confer Wnt dependency in pancreatic ductal adenocarcinoma. *Proc. Natl. Acad. Sci. USA* **110**, 12649–12654 (2013).
- Hsu, P.D., Lander, E.S. & Zhang, F. Development and applications of CRISPR-Cas9 for genome engineering. *Cell* **157**, 1262–1278 (2014).
- Hart, T. *et al.* High-Resolution CRISPR Screens Reveal Fitness Genes and Genotype-Specific Cancer Liabilities. *Cell* **163**, 1515–1526 (2015).
- Shalem, O. *et al.* Genome-scale CRISPR-Cas9 knockout screening in human cells. *Science* **343**, 84–87 (2014).
- Wang, T. *et al.* Identification and characterization of essential genes in the human genome. *Science* **350**, 1096–1101 (2015).
- Wang, T., Wei, J.J., Sabatini, D.M. & Lander, E.S. Genetic screens in human cells using the CRISPR-Cas9 system. *Science* **343**, 80–84 (2014).
- Hart, T. & Moffat, J. BAGEL: a computational framework for identifying essential genes from pooled library screens. *BMC Bioinformatics* **17**, 164 (2016).
- Hart, T., Brown, K.R., Sircoulomb, F., Rottapel, R. & Moffat, J. Measuring error rates in genomic perturbation screens: gold standards for human functional genomics. *Mol. Syst. Biol.* **10**, 733 (2014).
- Aguirre, A.J. *et al.* Genomic copy number dictates a gene-independent cell response to CRISPR/Cas9 targeting. *Cancer Discov.* **6**, 914–929 (2016).
- Brinkman, E.K., Chen, T., Amendola, M. & van Steensel, B. Easy quantitative assessment of genome editing by sequence trace decomposition. *Nucleic Acids Res.* **42**, e168 (2014).
- Persson, H. *et al.* CDR-H3 diversity is not required for antigen recognition by synthetic antibodies. *J. Mol. Biol.* **425**, 803–811 (2013).
- Gurney, A. *et al.* Wnt pathway inhibition via the targeting of Frizzled receptors results in decreased growth and tumorigenicity of human tumors. *Proc. Natl. Acad. Sci. USA* **109**, 11717–11722 (2012).
- Low, S.K. *et al.* Genome-wide association study of pancreatic cancer in Japanese population. *PLoS One* **5**, e11824 (2010).
- Jo, Y.S. *et al.* Frequent frameshift mutations in 2 mononucleotide repeats of *RNF43* gene and its regional heterogeneity in gastric and colorectal cancers. *Hum. Pathol.* **46**, 1640–1646 (2015).
- van de Wetering, M. *et al.* Prospective derivation of a living organoid biobank of colorectal cancer patients. *Cell* **161**, 933–945 (2015).
- Afekli, S., Pool, B., Schmerr, M., Penton, C. & Jensen, J. *Wnt7b* is required for epithelial progenitor growth and operates during epithelial-to-mesenchymal signaling in pancreatic development. *Dev. Biol.* **399**, 204–217 (2015).
- Arensman, M.D. *et al.* *WNT7B* mediates autocrine Wnt/ $\beta$ -catenin signaling and anchorage-independent growth in pancreatic adenocarcinoma. *Oncogene* **33**, 899–908 (2014).
- Dijksterhuis, J.P. *et al.* Systematic mapping of WNT-FZD protein interactions reveals functional selectivity by distinct WNT-FZD pairs. *J. Biol. Chem.* **290**, 6789–6798 (2015).

## ONLINE METHODS

**Plasmids.** Lenti Cas9-2A-BsdR vector (Addgene #73310) was used to generate cell lines stably expressing Cas9 and the pLCKO lentiviral vector (Addgene #73311) was used for TKO library construction and expression of individual gRNAs were described previously<sup>16</sup>. Each of the ten human FZD CRDs was cloned into the lentiviral expression plasmid pLenti-puro in the following cassette: FZD\_CRD-MYC-GPI. The lentiviral firefly luciferase construct (PGK-GFP-IRES-LUCIFERASE) used for generating HPAF-II-luc and AsPC1-luc cells for *in vivo* orthotopic model mice experiments was kindly supplied by the Ailles lab (Princess Margaret Cancer Centre, Department of Medical Biophysics, University of Toronto).

**Cell culture.** HPAF-II, PaTu8988S, PANC-1, HEK293T and mouse L-cell cell lines were maintained in DMEM containing 4.5 g/L D-glucose, L-glutamine (ThermoFisher #11965) and supplemented with 10% FBS (ThermoFisher) and Penicillin/Streptomycin (ThermoFisher #15140-163). AsPC-1, BxPC-3 and YAPC cell lines were maintained in RPMI 1640 with L-glutamine (ThermoFisher #11875) supplemented with 10% FBS and Penicillin/Streptomycin. CHO and patient derived cell lines (GP2A, GP3A, GP7B) were maintained in DMEM/F12 (ThermoFisher #11320-033) supplemented with 10% FBS and penicillin/streptomycin. All cell lines were maintained at 37° and 5% CO<sub>2</sub>. For puromycin selection, cells were selected in medium containing 2 µg/ml puromycin dihydrochloride (BioShop Canada #PUR333). For blasticidin selection, cells were selected in medium containing 10 µg/ml (HPAF-II), 8 µg/ml (PaTu8988S), 5 µg/ml (PANC-1), 2 µg/ml (BxPC-3) or 1 µg/ml (AsPC-1 and YAPC) of blasticidin hydrochloride (BioShop Canada #BLA477). Cells were tested for mycoplasma before screens and during follow-up studies using a MycoAlert mycoplasma detection kit (Lonza #LT07-118). HPAF-II, AsPC-1, PANC-1 and BxPC-3 cell lines were sourced from ATCC. PaTu8988S was a gift from F. Real, Madrid, Spain. Patient derived PDAC cell lines were generously provided by D. Hedley and M. Tsao, Toronto, Canada. All cell lines were authenticated with STR profiling at The Centre for Applied Genomics (Toronto, Ontario, Canada).

**Lentiviral gRNA library essentiality screens.** HPAF-II, AsPC-1 and PaTu8988S cell lines were transduced with Lenti Cas9-2A-BsdR as described above and selected with blasticidin. A polyclonal stable cell line was established and single clones were isolated by limited dilution. Clones were expanded and screened for Cas9 cleavage activity with a pLCKO delivered gRNA targeting FAM83G (**Supplementary Fig. 1b,e,h**). Briefly, this gRNA targets a SacII restriction site that is interrupted when indels are formed. Indel formation can be assessed by the ratio of undigested to digested PCR fragments. Clones were compared to their parental populations through viability assay and dose response sensitivity to the PORCN inhibitor, LGK974. Each clone was found to exhibit the same sensitivity as their parental population (**Supplementary Fig. 1c,f,i**).

The selected Cas9-2A-BsdR clone was transduced with the 90k gRNA library at an MOI of 0.3 and a library fold-coverage of 300x (~27 million transduced cells). 72 h post-infection (and 48 h post-puromycin selection) cells were split into two independent replicate populations of minimum 200-fold library coverage (18 million cells). In addition, T0 reference samples were collected (18 million cells) for genomic DNA extraction. Replicate populations were passaged in parallel every four days, with 18 million cells seeded over five 15 cm plates per population. Samples were collected at T15, T27, T31 and T35, at approximately 10, 18, 21 and 23 doublings respectively.

**Analysis of CRISPR negative selection screen.** Read counts for each gRNA were normalized for each replicate at each of the indicated time points (T27, T31, T35) and a log fold change relative to control (T0) was calculated for each gRNA with ≥30 reads in the T0 control sample. The BAGEL algorithm<sup>20</sup> was used to calculate a Bayes Factor for each gene, representing a confidence measure that the gene knockout results in a fitness defect. Bayes Factors at each time points were summed to a final BF for each gene. BAGEL software is available at <https://sourceforge.net/projects/bagel-for-knockout-screens/>.

**Analysis of previously published genome-wide CRISPR-Cas9 screen data.** Raw read count data from Aguirre *et al.*<sup>22</sup> were downloaded from <https://figshare.com/articles/AguirreMeyers/3420907>. Data from pancreatic cancer

cell lines were extracted and each replicate was normalized to a total of 10 million reads. gRNA sequences with < 30 reads in the control sample (pDNA\_pXPR003\_120K\_20140624) and gRNAs with the flag isUsed = FALSE in the file Achilles\_v3.3.8.reagent.table.txt were discarded. For all remaining guides (*n* = 65,721), a log<sub>2</sub> fold change was calculated relative to the control sample (a pseudocount of 0.5 reads was added to each sample), and BAGEL<sup>20</sup> was used to calculate a Bayes Factor of gene essentiality using all replicates for each cell line. Reference sets of essential and nonessential genes<sup>21</sup> were used to train BAGEL and to generate precision/recall curves.

**Crystal violet staining proliferation assay.** HPAF-II Cas9 cells were transduced with lentivirus generated with the indicated pLCKO plasmid as described above. 24 h after infection cells were treated with puromycin. After 48 h of selection, cells were PBS washed extensively, dissociated and counted. 2,000 cells per well were re-seeded in 24-well format in media without puromycin. 24 h post seeding, indicated wells were treated with DMSO control or 100 nM LGK-974 (Cayman Chemical #14072) (note that these wells were from the LacZ gRNA population). Medium was renewed every 3–4 days and cells were fixed, 10 days post plating, using 100% ice-cold methanol. After fixation cells were stained with 0.5% crystal violet, 25% methanol solution for 20 min at room temperature, after which staining solution was removed and plates were washed several times in dH<sub>2</sub>O. For Wnt3A conditioned media rescue experiment, cells were treated with 25% control or Wnt3A CM from initial infection onwards.

**Cell viability assays.** For FZD5/7 gRNA experiments, Cas9 expressing stable cell lines were transduced with indicated lentivirus as described above. 24 h after infection cells were treated with puromycin. After 48–72 h of puromycin selection, wells were washed with PBS extensively, dissociated and counted. Cells were re-seeded at 1,000 cells per well, six wells per gRNA, in 96 well plates. Medium was changed every 3–4 days and viability was measured with Alamar Blue (ThermoFisher #DAL1025) 7–11 days post plating. Briefly, 10 µl of Alamar Blue was added to 100 µl medium per well and incubated 1–4 h at 37°, 5% CO<sub>2</sub>. Fluorescence was measured at 560 nm excitation, 590 nm emission with Spectramax Gemini XS plate reader (Molecular Devices).

For antibody treatments, cells were seeded at 1,000–2,000 cells per well in 96-well plates. 24 h after seeding, cells were treated with antibodies in quadruplicate, at the indicated concentrations. Medium was changed and antibodies renewed after three days. Viability was measured with Alamar Blue, six days after plating, using the same procedure described above.

**Reverse transcription and quantitative real-time PCR.** After indicated treatments, cells were lysed in Tri-reagent (BioShop Canada #TSS120) and RNA extracted using the manufacturer's protocol. RNA concentration was quantified with Nanodrop1000 (Thermo Scientific) and 2 µg of RNA per sample was DNase I treated (ThermoFisher #AM2222). DNase treated RNA was used to make cDNA with High-Capacity cDNA Reverse Transcription Kit (ThermoFisher #4368813). Real-time PCR was performed using Power SYBR Green Master Mix on the 7900HT Fast Real-Time PCR system. Primer pairs are listed below. Analysis was done using the comparative cycle threshold (CT) method<sup>32</sup> with all samples normalized to *PPIB* (cyclophilin B) expression.

```

PPIB Forward: GGAGATGGCACAGGAGGAA
PPIB Reverse: GCCCGTAGTCAGTT
AXIN2 Forward: CTCCCCACCTTGAAATGAAGA
AXIN2 Reverse: TGGCTGGTCAAAGACATAG
NKD1 Forward: TGAGAACATGGAGAGAGTGAGCGA
NKD1 Reverse: GGTGACCTTGCCTGTTGTCAAA
MUC5AC Forward: AGCCGGAACCTACTACTCG
MUC5AC Reverse: AAGTGGTCATAGGCTCGTGC

```

**RNAseq analysis.** Gene level expression levels were derived from Klijn *et al.* (2015)<sup>33</sup>. Gene expression RPKMs were taken from supplementary data available at <http://research-pub.gene.com/KlijnEtAl2014/>.

**Isolation and characterization of Fabs against FZD.** The anti-FZD Fabs were isolated from a synthetic human Fab phage-displayed library (Library F)<sup>24</sup>.

Binding selections, phage ELISAs and Fab protein purification were performed as described<sup>34–36</sup>. Briefly, phage particles displaying the Fabs from Library F were cycled through rounds of panning with purified FZD-Fc fusion (R&D Systems) immobilized on 96-well Maxisorp Immunoplates (Fisher Scientific, Nepean, ON, Canada) as the capture target. After four rounds of selection, phage were produced from individual clones grown in a 96-well format and phage ELISAs were performed to detect specific binding clones. Clones with positive binding were subjected to DNA sequencing. The DNAs encoding for variable heavy- and light-chain domains of the positive binders were cloned into vectors designed for production of Fabs or light chain or IgG1 heavy chain, respectively, and Fabs were expressed from bacterial cells and IgGs from 293F cells (Invivogen, San Diego, CA, USA). Fab and IgG proteins were affinity-purified on Protein A affinity columns (GE Healthcare, Mississauga, ON, Canada).

**Immunofluorescence.** Cells were seeded in Cell carrierTM-96 well plates (PerkinElmer) and cultured overnight. Staining was performed with 200 nM Fabs diluted in PBS containing Ca<sup>2+</sup>/Mg<sup>2+</sup> in the presence of 5% donkey serum. Alexa Fluor488 AffiniPure F(ab')<sub>2</sub> was used as the secondary antibody (Jackson ImmunoResearch, catalog #109-546-097). Subsequently, cells were washed, fixed in 4% PFA and nuclei were stained with Hoechst 33342, trihydrochloride trihydrate solution (Molecular Probes). Cells were imaged on PerkinElmer Opera QEHS and acquired images were processed using Columbus software (CCBR, University of Toronto).

**Flow cytometry.** Primary staining of cells was performed with a 200 nM FZD profiler Fab. Alexa Fluor 488 AffiniPure F(ab')<sub>2</sub> was used as the secondary antibody (Jackson ImmunoResearch # 109-546-097). c-Myc (9E10) IgG1 (primary antibody, Santa Cruz, lot # D0306) and Alexa Fluor 488 IgG (secondary antibody, Life technologies, lot #1458649) were used as controls. Dead cells were excluded by staining with Fixable Viability Dye eFluor 660 (eBioscience, catalog number 65-0864). All reagents were used as per manufacturer's instructions. For cell-cycle analysis, cells were dissociated with trypsin and fixed with ethanol.  $1 \times 10^6$  fixed cells per samples were washed in PBS + 1% FBS solution and were stained with 50 µg/ml propidium iodide/50 µg/ml RNase A (ThermoFisher #EN0531) / 1% FBS in PBS solution and were subsequently subjected to Flow Cytometry. All flow cytometry was completed on BD FACSCanto II (BD Biosciences). Acquired data were analyzed with FlowJo Software (FlowJo, LLC).

**Mouse xenograft studies.** CB-17 Fox Chase SCID mice (six weeks old, female) were purchased from Charles River Laboratories (St. Constant, QC, Canada). The mice were housed in a pathogen-free environment at the animal facility at the University of Toronto. The study was conducted according to the guidelines of the Canadian Council on Animal Care (CCAC) and the animal use protocols approved by the University Animal Care Committee (UACC) at the University of Toronto.

The recombinant antibodies, IgG-2919 and OMP-18R5, were developed and purified as described above. Human γ-globulin was purchased from Jackson ImmunoResearch Laboratories, Inc. (West Grove, PA, USA), and Dulbecco's phosphate-buffered saline (DPBS, no calcium, no magnesium) was obtained from Thermo Fisher Scientific Inc. (Burlington, ON, Canada). Human γ-globulin and D-PBS were used as the experimental controls in this study.

To test the efficacy of the antibodies in subcutaneous tumor model, HPAF-II cells were inoculated subcutaneously (*s.c.*) into the right flank of mice with  $3 \times 10^6$  cells in DPBS injected per mouse. Tumor volumes were measured using vernier calipers and the mice were weighed twice weekly. Tumor volume was calculated using the formula:  $\frac{1}{2} (\text{Length} \times \text{Width}^2)$ . When tumors reached approximately 200 mm<sup>3</sup>, mice were randomly divided into four groups (9 or 10 mice/group) and the mean tumor volumes of each group were similar. Two mice with anomalously large or small tumors were excluded so that the mean tumor sizes of each group were very close before the treatment started. No mice were excluded after the treatment started. Each group received one of the following treatments: Human γ-globulin (10 mg/kg), DPBS (15 mL/kg), IgG-2919 (2 mg/kg) or IgG-2919 (1 mg/kg), twice weekly via intraperitoneal injection (*i.p.*) for four and a half weeks. For calculation of percentage of tumor growth inhibition (TGI), groups treated with antibody (Ab test) were compared with the group treated with human γ-globulin (control). TGI (%) was calculated

using the formula: TGI (%) = {(mean TVG control – mean TVG Ab test)/mean TVG control} × 100, where the mean TVG (tumor volume growth) = mean tumor volume at a defined study day – mean tumor volume the day of the first dosing.

To test the efficacy of the antibodies in orthotopic tumor models, HPAF-II or AsPC-1 cells stably expressing firefly luciferase were suspended in an ice-cold solution of 8.3 mg/mL Basement Membrane Extract (BME, Trevigen, Gaithersburg, MD) in DPBS. Mice were anesthetized by inhalation of isoflurane, and a 1.0 cm incision was made in the left upper abdominal flank. The pancreas along with the spleen was exposed and gently pulled out from peritoneal cavity. 50 µL of HPAF-II ( $1.5 \times 10^6$  cells/mouse) or AsPC1 ( $1 \times 10^6$  cells/mouse) cell suspension in the BME solution was carefully injected into the pancreatic tail, and the incision was closed with 4-0 absorbable suture. Mice were dosed with 0.1 mg/kg of Buprenorphine and 5 mg/kg of Ketoprofen *s.c.* 5 min before the surgery and once every 12 h for 3 days after the surgery. Tumors in the living animals were imaged by a 2D bioluminescence imaging system (In-Vivo Xtreme II, Bruker, Billerica, MA, USA) once every week from six (AsPC1 model) or seven (HPAF-II model) days after tumor cell inoculation, and the tumor images were analyzed by quantification of total photon flux of each tumor using Molecular Imaging Software (Bruker, Billerica, MA, USA). 24 mice bearing HPAF-II tumors were randomly divided into three groups (8 mice/group) 7 days after tumor cell inoculation and 27 mice bearing AsPC-1 tumors were randomly divided into 3 groups (9 mice/group) 6 days after tumor cell inoculation. The mean photon fluxes of the three cohorts with HPAF-II tumors were similar, as were the mean photon fluxes of the three cohorts with AsPC-1 tumors. Each group of the mice bearing HPAF-II tumors received one of the following treatments: DPBS (10 mL/kg), OMP-18R5 (2 mg/kg) or IgG-2919 (2 mg/kg), via *i.p.* twice weekly for three and a half weeks; each group of the mice bearing AsPC-1 tumors received one of the following treatments: DPBS (10 mL/kg), OMP-18R5 (5 mg/kg) or IgG-2919 (2 mg/kg) via *i.p.*, twice weekly for four weeks. Six mice from HPAF-II and four mice from AsPC-1 were excluded so that the mean fluxes of each group were similar after the first time imaging and before the treatment started. A single mouse in the HPAF-II vehicle control group was found deceased on day 32 of this study. Three mice bearing AsPC-1 tumors (one from each treatment group) died after the last imaging (day 34) due to failure to recover from anesthesia and the imaging procedure. For calculation of percentage of tumor growth inhibition (TGI), groups treated with antibody (Ab test) were compared with the group treated with DPBS (control). TGI (%) was calculated using the formula: TGI (%) = {(mean LucI control – mean LucI Ab test)/mean LucI control} × 100, where the mean LucI (photon flux Increase) = mean photon flux of the group at a defined study day – mean photon flux of the group the day of the first dosing. Investigators were not blinded for studies.

**Histological staining.** Tumor staining was carried out at the immunohistopathology and tissue processing lab at the University Health Network. Briefly, three representative tumors from each treatment group (human γ-globulin at 10 mg/kg, IgG-2919 at 1 mg/kg and IgG-2919 at 2 mg/kg) were embedded into a wax block and paraffin embedded tumors were cut into thin sections and mounted onto a microscope slide for routine staining with Hematoxylin and Eosin, Periodic Acid Schiff or PAS (Abcam – ab150680), Alcian Blue pH 1.0 (Abcam – ab150661), and Alcian Blue pH 2.5 (Abcam – ab150662). An Axioscan slide scanner system was used to generate high resolution digital images of the whole tumor sections at 40× in brightfield mode, and the images were exported as .png files using ZEN software.

**Colorectal cancer organoid studies.** Organoid lines derived from CRC patients are identified, as previously reported<sup>28</sup>, as P14T and P18T (APC mutant) and P19TB (RNF43 mutant). The organoid lines were expanded and processed as described previously<sup>28</sup>. P1947 is a clonal organoid line that was generated and cultured in the same way as previously described<sup>28</sup>. Briefly, the resected tumor was subdivided in different pieces and organoids established were dissociated into single cells by trypsinization, and sorted by FACS without using any antibodies. Around 50 sorted cells were embedded into 10 µL of Basement Membrane matrix (BME, Amsbio) in 96 well-plate and left to grow. Established clonal organoids were trypsinized by using TrypLE (Thermo Fisher Scientific) and expanded in order to generate a clonal line.

In order to perform a cell viability test using Cell Titer-Glo 3D (Promega), organoids were filtered through a 40  $\mu\text{m}$  filter and were seeded in 384 well plates (coated with BME). ~500 organoids were resuspended in a total volume of 40  $\mu\text{l}$  of medium (with 5% BME) per well. Importantly, the culture medium did not contain Wnt. IWP2 (a PORCN inhibitor) and antibodies were distributed using a Tecan D300 Digital Dispenser. Organoids were exposed to an 8-point dilution series for each antibody and one fixed concentration of IWP2 (1  $\mu\text{M}$ ). Fresh drug and antibodies were added at day 0. As internal controls, we used DMSO and Staurosporin (2  $\mu\text{M}$ ) in order to normalize the data (DMSO values as 100% survival and Staurosporin values as 0% survival).

After 4 days, 40  $\mu\text{l}$  of Cell Titer-Glo 3D was added, plates were shaken for 5 min, incubated for an additional 25 min and centrifuged before luminescence measurement.

In each experiment, all conditions were run in triplicate and at least three biological replicates were run per organoid line. DMSO was added to all wells to normalize to the highest concentration (0.1% for DMSO in Staurosporin control). For analysis, the data was sorted and normalized to the positive control (Staurosporin) and the Negative control (DMSO). Essentially, for each organoid line the average value for Staurosporin was subtracted from all of the values, and these were divided by the resulting average of the DMSO condition.

**Statistical analysis.** All statistical analyses were completed with Graphpad Prism 6 (GraphPad Software, La Jolla, California, USA). For gRNA based viability assays and RT-qPCR in **Figure 2**, each experiment was normalized to *LacZ*

control values. Statistical analysis of multiple independent experiments was completed by one-sample *t*-test, compared to a hypothetical value of one. For two-tailed unpaired *t*-tests in cell lines, data from multiple independent experiments was assumed to be normally distributed and of equal variance. No statistical method was used to pre-determine sample size. For mouse xenograft studies, tumor sizes and weights were confirmed to be of standard distribution with D'Agostino and Pearson normality test. In some cases, data was not normally distributed and Mann-Whitney *U* test was used. *F*-test was used to verify equal variances. In some cases, 2 mg/kg IgG-2919 treatment group had significantly different variance, so Welch's correction was applied to *t*-test. Sample size was chosen to have adequate confidence in the mean.

32. Bookout, A.L., Cummins, C.L., Mangelsdorf, D.J., Pesola, J.M. & Kramer, M.F. High-throughput real-time quantitative reverse transcription PCR. *Curr. Protoc. Mol. Biol.* **73**, 15.18.1–15.8.28 (2006).
33. Klijn, C. et al. A comprehensive transcriptional portrait of human cancer cell lines. *Nat. Biotechnol.* **33**, 306–312 (2015).
34. Colwill, K. Renewable Protein Binder Working Group & Graslund, S. A roadmap to generate renewable protein binders to the human proteome. *Nat. Methods* **8**, 551–558 (2011).
35. Fellouse, F.A. et al. High-throughput generation of synthetic antibodies from highly functional minimalist phage-displayed libraries. *J. Mol. Biol.* **373**, 924–940 (2007).
36. Rajan, S. & Sidhu, S.S. Simplified synthetic antibody libraries. *Methods Enzymol.* **502**, 3–23 (2012).

## Corrigendum: Host DNA released by NETosis promotes rhinovirus-induced type-2 allergic asthma exacerbation

Marie Toussaint, David J Jackson, Dawid Swieboda, Anabel Guedán, Theodora-Dorita Tsourouktsoglou, Yee Man Ching, Coraline Radermecker, Heidi Makrinioti, Julia Aniscenko, Michael R Edwards, Roberto Solari, Frédéric Farnir, Venizelos Papayannopoulos, Fabrice Bureau, Thomas Marichal & Sebastian L Johnston  
*Nat. Med.* 23, 681–691 (2017); published online 1 May 2017; corrected after print 12 July 2017

In the version of this article initially published, Dr. Nathan W Bartlett was inadvertently omitted from the author list and the Contributions section. The errors have been corrected in the HTML and PDF versions of the article.

## Corrigendum: The cold-induced lipokine 12,13-diHOME promotes fatty acid transport into brown adipose tissue

Matthew D Lynes, Luiz O Leiria, Morten Lundh, Alexander Bartelt, Farnaz Shamsi, Tian Lian Huang, Hirokazu Takahashi, Michael F Hirshman, Christian Schlein, Alexandra Lee, Lisa A Baer, Francis J May, Fei Gao, Niven R Narain, Emily Y Chen, Michael A Kiebish, Aaron M Cypess, Matthias Blüher, Laurie J Goodyear, Gökhan S Hotamisligil, Kristin I Stanford & Yu-Hua Tseng  
*Nat. Med.* 23, 631–637 (2017); published online 27 March 2017; corrected after print 23 August 2017

In the phrase, “Here we show that the lipid 12,13-dihydroxy-9Z-octadecenoic acid (12,13-diHOME) is a stimulator of BAT activity, and that its levels are negatively correlated with body-mass index and insulin sensitivity,” located in the abstract, the word “resistance” should take the place of the word “sensitivity”.

Also, the authors have clarified in more detail how the FATP1 oligomer density was quantitated in Figure 4f. This information can be found in the “Membrane Fractionation” section of the Online Methods: “To quantify FATP1 in scanned immunoblots, regions of interest of identical size were drawn in each lane at the same molecular weight, and integrated pixel density was measured using ImageJ software. For each independent experimental replicate, the integrated pixel density for each lane was expressed normalized to the control lane, or in the case of the experimental replicate with two control lanes, the integrated pixel density for each lane was expressed normalized to the average of both control lanes. The data are expressed as the average normalized value for each lane, with the error bars representing s.e.m.”

## Corrigendum: Targeting cellular senescence prevents age-related bone loss in mice

Joshua N Farr, Ming Xu, Megan M Weivoda, David G Monroe, Daniel G Fraser, Jennifer L Onken, Brittany A Negley, Jad G Sfeir, Mikolaj B Ogródnik, Christine M Hachfeld, Nathan K LeBrasseur, Matthew T Drake, Robert J Pignolo, Tamar Pirtskhala, Tamara Tchkonia, Merry Jo Oursler, James L Kirkland & Sundeep Khosla  
*Nat. Med.* 23, 1072–1079 (2017); published online 21 August 2017; corrected after print 11 October 2017

In the version of this article initially published, the representative images in Fig. 2n were inadvertently duplicated in Fig. 4h. A correct version of the images for Fig. 4h has been supplied. The authors wish to point out that this error did not affect the other data reported in the paper or the conclusions drawn. The error has been corrected in the HTML and PDF versions of the article.

## Corrigendum: Genome-wide CRISPR screens reveal a Wnt–FZD5 signaling circuit as a druggable vulnerability of *RNF43*-mutant pancreatic tumors

Zachary Steinhart, Zvezdan Pavlovic, Megha Chandrashekhar, Traver Hart, Xiaowei Wang, Xiaoyu Zhang, Mélanie Robitaille, Kevin R Brown, Sridevi Jaksani, René Overmeer, Sylvia F Boj, Jarrett Adams, James Pan, Hans Clevers, Sachdev Sidhu, Jason Moffat & Stéphane Angers  
*Nat. Med.* 23, 60–68 (2017); published online 21 November 2016; corrected after print 20 September 2017

In the version of this article initially published, duplicate panels in Figure 5e were incorrectly used in the assembly of the figure, for which all original panels are presented in Supplementary Figure 10. The errors in Figure 5e have been corrected in the HTML and PDF versions of the article.